The GZK Feature in our Neighborhood of the Universe

Michael Blanton [a], Pasquale Blasi [a] Angela V. Olinto [b,1],

[a]*Fermi National Accelerator Laboratory, Batavia, IL 60510-0500*

[b]*Department of Astronomy & Astrophysics, & Enrico Fermi Institute,
The University of Chicago, Chicago, IL 60637*

Abstract

We calculate numerically the spectrum of ultra-high energy cosmic rays on Earth assuming that their sources are distributed in space like the observed galaxies. We use the CfA2 and the PSCz galaxy redshift surveys to model the local galaxy distribution, properly taking into account the galaxy selection functions for each survey. When the survey selection effects are included, we find that the local overdensity is only a factor of two, an order of magnitude less than used in some earlier studies. An overdensity of two is not enough to bridge the gap between the predicted number of events above 10^{20} eV and the measured flux at these highest energies. This conclusion is particularly strong for soft injection spectra ($\propto E^{-3}$) where the observed number of events is 6 σ higher than the expected one. However, if the injection spectrum is hard ($\propto E^{-2}$), the small local overdensity helps bring the present data within 2σ of the low number of events predicted above 10^{20} eV. In this case, the Greisen-Zatzepin-Kuzmin cutoff is not a *cutoff* but rather a *feature* in the cosmic ray spectrum.

Key words: Cosmic Rays, Ultra-high energy, Propagation, Acceleration
PACS: 96.40.- zv, 95.85.Ry, 13.85.Tp

1 Introduction

The unexpected detection of cosmic rays with energies above 10^{20} eV has triggered considerable interest in the possible origin and nature of these particles [1]. These highest energy events are surprising for the following reasons. If these particles are protons, they likely originate in extragalactic sources,

---

[1] Corresponding author. E-mail: olinto@oddjob.uchicago.edu

since at these high energies the Galactic magnetic field cannot confine protons in the Galaxy. However, extragalactic protons with energies above a few times 10^{19} eV can produce pions through interactions with the cosmic microwave background (CMB) and consequently lose significant amounts of energy as they traverse intergalactic distances [2]. Therefore, in addition to the extraordinary energy requirements for astrophysical sources to accelerate protons to $\gtrsim 10^{20}$ eV, the photopion threshold reaction suppresses the observable flux above $\sim 10^{20}$ eV. These conditions were expected to cause a natural high-energy limit to the cosmic ray spectrum known as the Greisen-Zatsepin-Kuzmin (GZK) cutoff [2].

As clearly shown by the most recent compilation of the AGASA collaboration data [3], the spectrum of cosmic rays does not end at the expected GZK cutoff. The significant flux observed above 10^{20} eV together with a nearly isotropic distribution of event arrival directions has challenged astrophysically based scenarios (see e.g., [4] and references therein) and has inspired a number of alternatives (see, e.g., [5] and references therein). However, the GZK cutoff is not an absolute *end* to the cosmic ray spectrum but it generates a *feature* around 5×10^{19} eV. The spectrum recovers at energies above this feature [6] and the local distribution of sources can significantly affect the agreement between predicted and observed spectra. In particular, a local overdensity of sources can decrease the gap between observed and detected events above the GZK cutoff [7–9]. This effect can easily be understood: photopion energy losses limit the maximum distance at which sources can contribute at the highest energies to a few tens of Mpc, while cosmic rays below the pion production threshold come from much larger volumes. A local overdensity will increase the observed flux at the highest energies relative to the lower energy flux. Here we show that the observed local overdensity is not high enough to explain the data unless, perhaps, the sources have a hard injection spectrum.

In the following, we simulate the propagation of ultra-high energy cosmic rays (UHECRs) from extragalactic sources to Earth. Our numerical propagation code includes pair production, photopion production, and adiabatic losses due to the universe's expansion. For a uniform distribution of sources, our numerical results agree well with previous results and analytical calculations. We study the effect of a local overdensity by assuming that the number density of sources is proportional to the number density of galaxies. To keep this study independent of specific hypothetical sources, we use different injection spectra and consider a possible source evolution with redshift. However, since we assume that UHECRs are protons, our results are mostly relevant for extragalactic astrophysical acceleration scenarios.

Rather than adopting analytic models of the galaxy distribution, as do [9,10], we extract the distribution of galaxies from observations of large scale structure using the CfA2 and the PSCz galaxy catalogs. We assume that the den-

sity field derived from these studies has the same shape as the density field of UHECR sources, although *a priori* UHECR sources may cluster differently from luminous matter. We show that the local density is only about a factor of two above the mean, in contrast with much higher estimates previously published [8]. This large discrepancy was caused by neglecting the necessary galaxy selection functions which account for the fact that nearby galaxies are far easier to detect than far away galaxies. Once we include the selection functions, we find that the real overdensity is not high enough to bridge the gap between predicted and observed spectra for soft sources ($J(E) \propto E^{-\gamma}$, with $\gamma = 3$). However, sources with a hard injection spectrum ($\gamma \lesssim 2.1$) can fit the present data within 2σ, at energies above a few 10^{19} eV. Sources of UHECRs distributed as ordinary galaxies are marginally consistent with present data and, for hard injection spectra, the GZK cutoff is not really a *cutoff* but a *feature* in the high-energy cosmic ray spectrum.

The plan of this paper is as follows. In §2, we discuss the proper way to model a distribution of sources associated with galaxies. We derive the galaxy density field in our neighborhood of the universe using the CfA2 and PSCz galaxy redshift surveys with their respective selection function. In §3, we describe our UHECR propagation code. In §4, we display the results for different injection spectra and a realistic spatial distribution of sources. We also contrast our results with previous work and analytical estimates. We conclude in §5.

2 The Galaxy Density Field

Although galaxies are not homogeneously distributed in the local universe, the GZK cutoff is usually calculated assuming a homogeneous distribution of sources throughout space. If the sources are distributed like the luminous matter around us, the effects of an inhomogeneous galaxy distribution needs to be taken into account when predicting the spectrum of UHECRs. In order to include the effects of the spatial inhomogeneity in the UHECR spectrum, we must consider the estimated galaxy density field in our neighborhood of the universe. The density field is usually measured by selecting galaxies from an imaging survey of the sky and taking their redshifts. Almost invariably, the galaxies are selected to be brighter than some limiting flux in some band, f_{lim}, expressed as an "apparent magnitude," $m_{\mathrm{lim}} = -2.5 \log_{10}(f_{\mathrm{lim}}/f_0)$, where f_0 is an arbitrary zero-point. For all (or for some random subsample) of the galaxies brighter than this, one takes their spectra and determines their redshifts z. According to the Hubble law, the redshifts are related to their distances $d = H_0 cz$, where c is the speed of light and $H_0 \equiv 100h$ Mpc/ km/s, with $h \approx 0.5$–0.8 (*e.g.*, [11]).

However, a flux-limited survey is not a volume-limited survey. In a flux-limited

survey, the raw distribution of redshifts cannot be used without regard to the way galaxies were selected. Here we describe the proper way to derive density fields from galaxy redshift surveys. We limit ourselves to measuring the density in redshift space and do not include the small effects of deviations from the Hubble law due to galaxy peculiar velocities. We base our approach on methods dating back to [12] (see, e.g., [13] for a recent review).

We will use two surveys for our analysis. To compare directly with [8], we consider the Center for Astrophysics Redshift Survey (CfA2; [14]). Although this survey comprises about 10,000 galaxy redshifts (selected to be brighter than $m = 15.5$, a B-band magnitude), it covers only about 17% of the whole sky. In order to better evaluate the effects of the density field of galaxies on the cosmic ray spectrum, we should use surveys which probe the density field over nearly the whole sky. The best sample of galaxies to use for this purpose is the IRAS PSCz Survey [15], which consists of about 15,000 galaxies with infrared fluxes > 0.6 Jy and covers about 84% of the sky.

A consequence of the flux limits in any survey is that at different redshifts, a different set of galaxy luminosities L is observed, determined by the faintest luminosity observable at that redshift $L_{\min}(z)$. For an Euclidean metric, this luminosity is related to the flux limit by:

$$L_{\min}(z) = 4\pi (H_0 c z)^2 f_{\lim}. \tag{1}$$

At cosmological distances (generally only appropriate when $z > 0.1$) more complicated relations apply, which in general depend on the cosmological model [16] (see [17] for a useful compilation of results). If the distribution of galaxy luminosities is described by the galaxy luminosity function $\Phi(L)$, then the fraction of all galaxies that are observable at any redshift is given by:

$$\phi(z) = \frac{\int_{L_{\min}(z)}^{\infty} dL \ \Phi(L)}{\int_0^{\infty} dL \ \Phi(L)}. \tag{2}$$

The quantity $\phi(z)$ is usually referred to in the literature as the "selection function" [18]. The most common methods used to determine the galaxy luminosity function from the survey itself are those of [19] and [20]. These methods assume that the luminosity function is universal (i.e., independent of redshift) and use nearby galaxies to determine the shape of the faint end and far away galaxies for the shape of the bright end.

Consider, for example, Figure 1, which shows in the top panel the distribution of galaxies and redshifts in CfA2. Here we express galaxy luminosity in terms of the "absolute magnitude," $M = -2.5 \log_{10} L+$ const; thus, in the figure, the faintest galaxies are at the top. The thick solid line shows the flux limit of the

survey, translated into an absolute magnitude limit at each redshift. Because of this limit a number of galaxies which are observable at low redshifts are too faint to be observed at higher redshift. The fraction of galaxies $\phi(z)$ between absolute magnitudes $-22 < M < -10$ which are unobservable at each redshift is shown in the bottom panel of Figure 1, based on a fit to the luminosity function in the survey using the method of [19]. Because the function falls rapidly from unity, it is clear that even at low redshifts the effects of the flux limit are important.
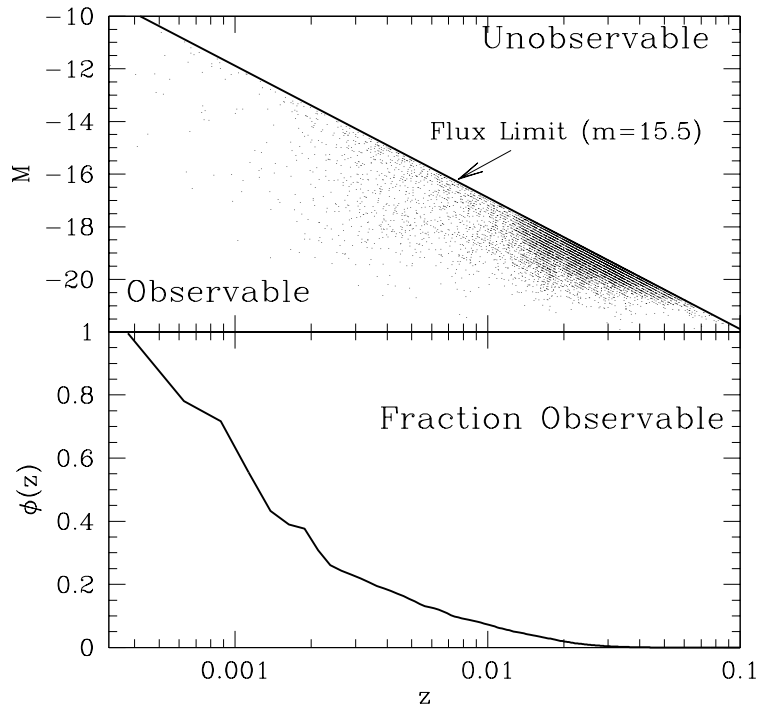

Fig. 1. *The top panel shows the absolute magnitudes (related to luminosity by $M = -2.5 \log_{10} L +$ const) and redshifts of CfA2 galaxies. Shown as the thick solid line is the flux limit, converted to the appropriate absolute magnitude at each redshift. The bottom panel shows the fraction of galaxies in the range $-22 < M < -10$ that we estimate to be brighter than the flux limit. This function falls rapidly with redshift. When interpreting the top plot, remember that the volume probed at low redshift is far smaller than that probed at high redshift.*

In principle, we can construct a volume-limited sample by choosing only galaxies brighter than some magnitude M up to the redshift at which the thick solid line representing the flux limit crosses M. This usually decreases significantly the number of galaxies and the redshift depth of the survey. A more effective approach is to use $\phi(z)$ to calculate the distribution of observed galaxies with redshift which one would expect if the distribution were homogeneous. Then, the density field can be inferred by comparing the actual counts to these

expected counts. The top panel of Figure 2 compares these expected counts (dotted line) in redshift shells of thickness 0.001 to the observed counts (solid line) in CfA2. It appears that locally we are in an overdensity of galaxies of about a factor of two; note that at large distances, where each shell corresponds to a considerable amount of volume, and thus averages over large-scale structures, the number of galaxies is very nearly the expected number. Instead, if the flux limit is neglected (dashed line), the "expected" number of galaxies in each shell scales approximately as the square of the redshift of that shell. If we normalize these "expected" counts in approximately the same way as [8], we recover the incorrect result that we live in an overdensity of approximately a factor of 30. It is clear from the comparison of the dotted to the dashed curve that neglecting the flux limits is a poor approximation. Put simply, we do not live in a large overdensity, but we can certainly detect galaxies more easily if they are close by rather than far away.
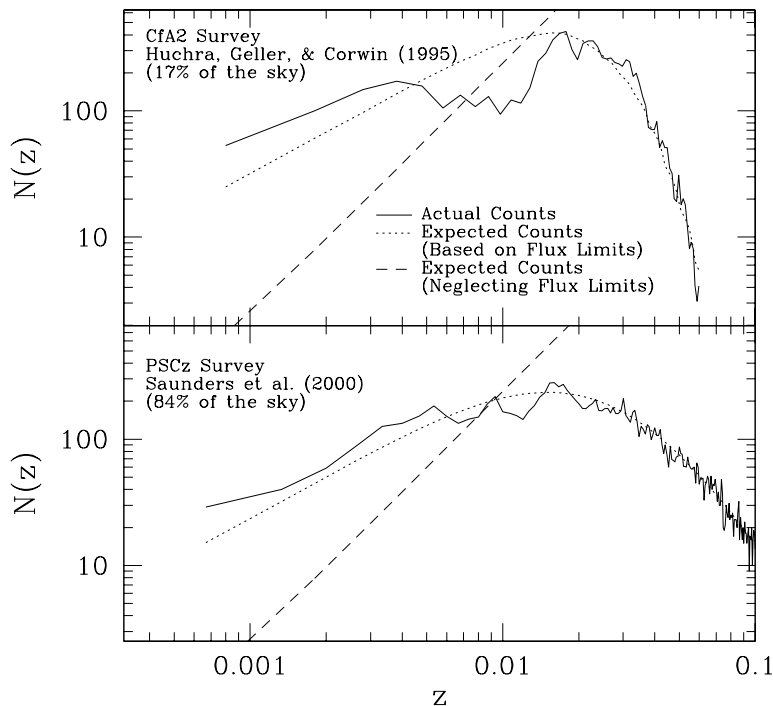

Fig. 2. *Comparison of observed counts (solid line) to those predicted based on the flux limits (dotted line) and those predicted neglecting the flux limits (dashed line). The CfA2 survey is shown at top, the PSCz at bottom. Both show a local overdensity of only about a factor of two when the flux limits are properly accounted for.*

As mentioned above, the CfA2 survey covers a relatively small fraction of the sky. Thus, the PSCz redshift survey provides a more useful sample to use in the context of this paper. Using the selection function provided by [15], we

again show the expected versus the observed counts for the PSCz survey in the bottom panel of Figure 2. This survey also shows we are living in a slight overdensity, and furthermore reveals the general homogeneity of the nearby universe. (The actual counts and their dependence on redshift are different from CfA2, because the galaxies are selected in different ways).

3 The Propagation Code for UHECRs

Armed with a more realistic model of the local universe, we can calculate the spectrum of UHECRs that would be observed on Earth for extragalactic sources with different injection spectra. Our numerical propagation code includes pair production and photopion production as energy losses, as well as adiabatic losses due to the expansion of the universe. We compare our numerical results with analytical calculations which we carry out as in [6]. In order to isolate the effect of density inhomogeneities we neglect the effect of magnetic fields in this paper.

We compare the results of the simulations with the observed spectrum by requiring that the total number of simulated events with energy above a normalizing energy, E_{norm}, be the same as what is observed. In general we choose $E_{norm} \simeq 10^{19}$ eV since at lower energies the flux of cosmic rays is likely to have a galactic origin and at higher energies the observed number of events is very small. For a given source spectral index, we generate many realizations of the spectrum on Earth. Each realization has the same total number of observed particles above E_{norm} calculated as follows. The flux of UHECRs contributed from a shell of thickness Δz at redshift z is proportional to $p(z) \propto (1+z)^{m-5/2} f(z)$, where the redshift dependence of the density of sources and the flux suppression due to distance are included explicitly [21]. In this formula, we allow for source luminosity evolution through the parameter m. The function $f(z)$ describes possible deviations from a homogeneous spatial distribution of sources. For a homogeneous distribution $f(z) = 1$, otherwise $f(z)$ represents the local overdensity of sources at redshift z as, for example, those derived from the catalogs introduced in §2. We assign the redshift of one event by extracting a random number according to the distribution $p(z)$ given above. The energy of the particle at the source is extracted from a distribution representing the spectrum of the source assumed to have the form of a power law $E^{-\gamma}$. The particle is then propagated from the source to the detector.

The photopion energy losses are simulated following [22]. In each spatial step of the simulation of size Δs (~ 200 kpc), the average number of photons that can induce the production of pions in the scattering with a proton of energy

E at time t is

$$\langle N_{ph}(E, \Delta s)\rangle = \frac{\Delta s}{K_p(E)l(E)}. \qquad (3)$$

Here, $l(E) = c\left[(1/E)(dE/dt)\right]^{-1}$ is taken from [6] and $K_p(E)$ is an effective inelasticity at energy E, which can be approximated by

$$K_p(E) \simeq 0.2\left(\frac{E_{th} + 2.5E}{E_{th} + E}\right), \qquad (4)$$

with $E_{th} = 3 \times 10^{11}$ GeV [22]. Once the average number of pion producing photons has been determined over the path Δs, the actual number of photons with which the proton interacts is extracted from a Poisson distribution with mean $\langle N_{ph}(E, \Delta s)\rangle$. For sufficiently small Δs, the number of photons in each step is usually either zero or one. The energy of each photon is extracted from a Planck distribution at temperature $T_{CMB} = 2.728$ K (with a minimum energy corresponding to the threshold for pion production). Since the CMB photons are isotropically distributed in space, we extract the interaction angle from a flat distribution in $\cos(\theta)$. The final energy of the proton after each scattering with a CMB photon is calculated from the kinematics of the scattering. Since the inelasticity for pair production is very low, we treat it as a continuous energy loss process.

We compare our numerical results with analytic results for the modification factor from single sources and from a distribution of sources as in [6]. The agreement is excellent and the effect of the fluctuations at energies larger than $\sim (3-4) \times 10^{19}$ eV is evident in Figures 5–8 as we discuss below. The average of the simulated flux is slightly larger than the analytic one, as expected for the stochastic process of photopion production (on small distances there is an appreciable chance that some protons do not interact at all).

4   Results

As we stressed above, a local overdensity increases the observed flux above GZK energies with respect to the flux at lower energies. To show this effect clearly, we estimated the change in the spectrum due to a simple top-hat model before considering more realistic models of the galaxy density field. In Figure 3, we display the results of our analytical calculation for three choices of the overdensity, $\rho/\bar{\rho} = 1$, 10, 30 (solid, dashed, and dash-dotted lines respectively), all in a volume of radius ~ 20 Mpc around the Earth and with source spectral index $\gamma = 3$. From this figure, it is clear that the overdensity

increases the flux at the highest energies versus the flux at and below the GZK feature, as mentioned above.
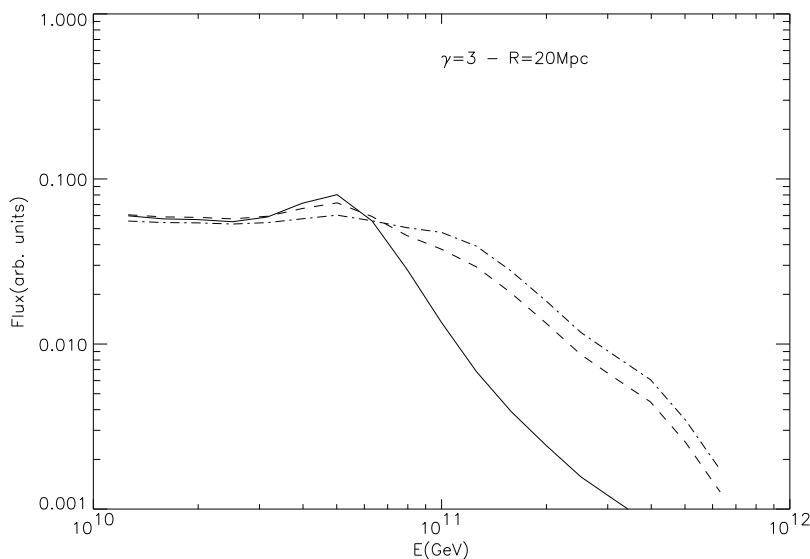

Fig. 3. *The effect of a local overdensity within* 20 *Mpc on the fluxes of UHE-CRs, according to our analytical calculation for three choices of the overdensity,* $\rho/\bar{\rho} = 1,\ 10,\ 30$ *(solid, dashed and dash-dotted lines respectively), all in a volume of radius* ~ 20 *Mpc around the Earth and with source spectral index* $\gamma = 3$.

The galaxy surveys discussed in §2 provide a more realistic model of the local density field. Among the different surveys, the PSCz catalog covers a lot more solid angle and reaches further (up to a redshift $z_{max} = 0.1$) when compared to the CfA2 survey. Thus, we use the PSCz to study the effect of different source spectra below. But first we compare the results of the two catalogs for a fixed spectral index ($\gamma = 3$) with the homogeneous distribution in Figure 4. This choice of γ allows a direct comparison of our results with those of [8]. In this figure, we normalize the spectrum by requiring that the number of events with energy above 10^{19} eV equal the AGASA number of 728 [23,24]. The error bars in the simulation are obtained by generating 100 realizations and calculating the mean and variance of the set. Figure 4 shows that the two catalogs give very similar results.

In Figure 5, we compare the case of a homogeneous distribution and the PSCz catalog versus the AGASA data also for $\gamma = 3$. The total number of events with $E > 10^{20}$ eV is 1.2 ± 1.0 for the homogeneous case and 1.5 ± 1.0 for the PSCz catalog of galaxies. Both numbers are consistent with 1, while AGASA has detected 8 events with $E > 10^{20}$ eV. The data is more than 6 σ away from the observations. None of our realizations have the observed number of events for this soft spectrum. In the figure, the solid and dashed lines represent the result of the analytical calculations for the same value of the parameters and for the homogeneous and PSCz cases respectively. The dash-dotted and dash-
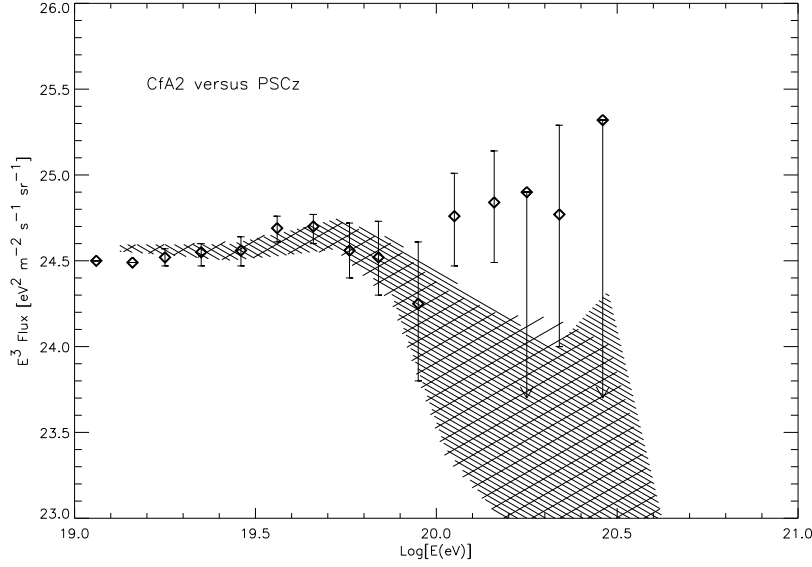
Fig. 4. *Simulated fluxes of UHECRs for $\gamma = 3$ using the CfA2 catalog (hatched upwards to the right, i.e., like "/") and the PSCz catalog (hatched downwards to the right, i.e., like "\").*

dot-dot-dotted lines trace the mean simulated fluxes for the homogeneous case (hatched downwards to the right, i.e., like "\") and the PSCz case (hatched upwards to the right, i.e., like "/"). As can be seen from Figure 5, the difference between the analytic calculations and the mean of the numerical calculation is quite small. In addition, the homogeneous case has only slightly lower fluxes at higher energies than the realistic models. Here our results differ significantly from those of [8], due to the fact that the real local overdensity is much smaller than found in [8].

In Figure 6, we show the generated fluxes assuming that 9075 events have been observed above 10^{19} eV, a number which the Auger project is expected to reach in the first 3 years of operation. Again we compare the results of a homogeneous distribution of sources (\ hatches) with those associated with the PSCz galaxy distribution (/ hatches), using $\gamma = 3$ for both. As expected from a larger sample, the size of the error bars decreases significantly. The number of events at $E > 10^{20}$ eV in the two cases is still much smaller than if extrapolated from the AGASA observations (~ 100). This figure shows that the Auger project will be able to constrain the nature of the GZK feature much more accurately than possible at present.

It is clear that with a source injection spectrum as steep as $\gamma = 3$, the number of events with $E > 10^{20}$ eV is significantly smaller than what has been observed so far. Since sources with harder spectra have been proposed, we consider different choices for the injection spectrum. We simulated the case of $\gamma = 2.7$, but the results do not diffr significantly from the $\gamma = 3$ case. Next we discuss
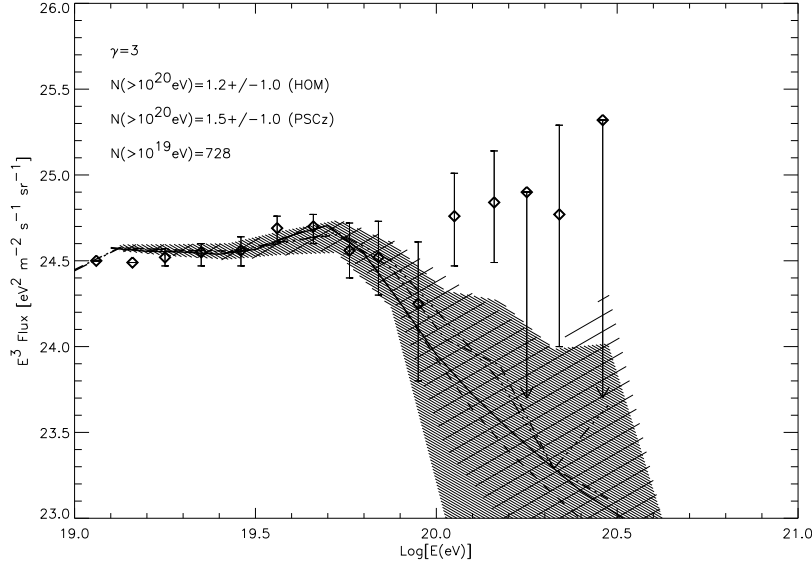
Fig. 5. *Simulated fluxes for the AGASA statistics of 728 events above 10^{19} eV, and $\gamma = 3$, using a homogeneous source distribution ($\backslash$ hatches) and the PSCz distribution (/ hatches). The solid and dashed lines are the results of the analytical calculations for the same two cases. The dash-dotted and dash-dot-dot-dotted lines trace the mean simulated fluxes for the homogeneous and the PSCz cases.*

the case of $\gamma = 2.1$, where we find the gap between observed and predicted flux to reach the 2 σ level.

In Figure 7, we show the results for $\gamma = 2.1$ for three cases: a homogeneous distribution of the sources with $z_{max} = 0.1$ (/ hatches), the PSCz distribution with $z_{max} = 0.1$ (horizontal hatches), and a homogeneous distribution with $z_{max} = 1$ ($\backslash$ hatches). For such hard spectra, we need to adjust the normalization energy, E_{norm}, such that the flux at energies below 10^{20} eV is consistent with observations in this energy range. Thus, we choose the normalization energy, $E_{norm} = 4 \times 10^{19}$ eV, where the number of events observed by AGASA [24] (49) is still statistically significant.

Again, Figure 7 shows that the number of events at $E > 10^{20}$ eV is affected by the local distribution of the sources. For the adopted normalization, the homogeneous distribution gives 3.3 ± 1.6 events above 10^{20} eV (to be compared with the observed 8) and the PSCz distribution provides 3.7 ± 2.0 events in the same range. In this last case, about 5% of our realizations give a number of events above 10^{20} eV which is equal or larger that the observed one (consistent with a 2σ significance for a Gaussian error distribution).

The deficit of events at energies lower than $\sim (3-4) \times 10^{19}$ eV for hard spectra is evident in the case of $z_{max} = 0.1$. Since the high redshift sources contribute mainly to the low energy flux, we also considered the case where the maximum redshift is $z_{max} = 1$. The increase in z_{max} moves the deficit to energies lower
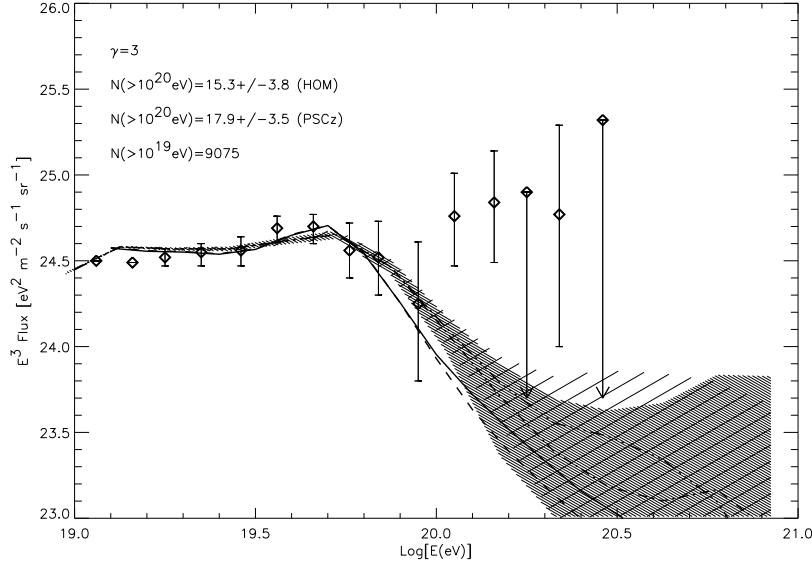
11

Fig. 6. *Simulated fluxes for the Auger projected statistics of 9075 events above 10^{19} eV, and $\gamma = 3$, using a homogeneous source distribution ($\backslash$ hatches) and the PSCz distribution (/ hatches). The solid and dashed lines are the results of the analytical calculations for the same two cases. The dash-dotted and dash-dot-dot-dotted lines trace the mean simulated fluxes for the homogeneous and the PSCz cases.*
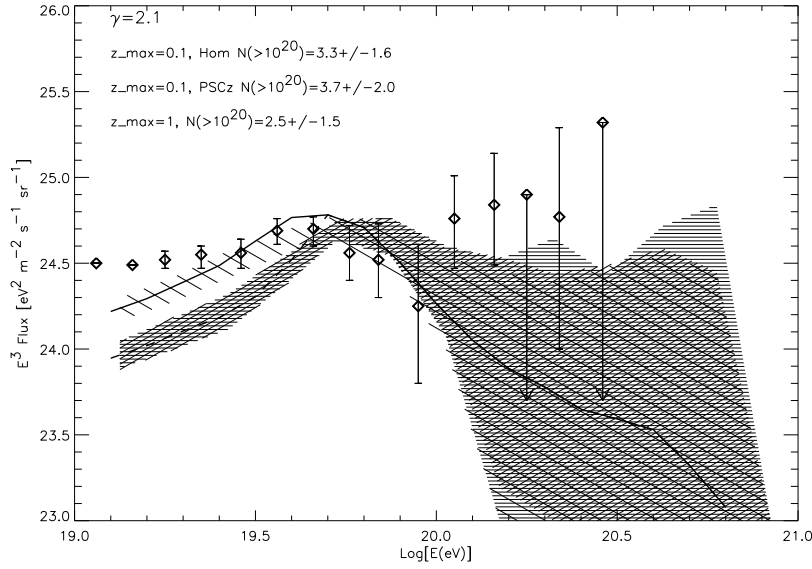

Fig. 7. *Simulated fluxes for the AGASA statistics of 728 events above 10^{19} eV, and $\gamma = 2.1$, using a homogeneous source distribution with $z_{max} = 0.1$ (/ hatches), the PSCz distribution with $z_{max} = 0.1$ (horizontal hatches), and a homogeneous source distribution with $z_{max} = 1$ ($\backslash$ hatches).*

than $\sim 2 \times 10^{19}$ eV, as shown in Figure 7 (the discrepancy is about a factor 1.6).

We also considered the effect of a source luminosity evolution. For instance, if the luminosity of the sources increases with redshift z, the flux of UHECRs at energies below the GZK cutoff will also increase. This is shown in Figure 8 for the case $m = 0$ (horizontal hatches), $m = 2$ (/ hatches), and $m = 4$ (\ hatches). This type of source evolution by itself does not improve significantly the agreement between the theoretical prediction and the AGASA data at low energies, leaving unaltered the number of events above 10^{20} eV. In fact the height of the bump at $\sim (3 - 4) \times 10^{19}$ eV also increases with large values of m, thus reducing the number of events with energy larger than 10^{20} eV when the number of events is normalized to the integral flux above 4×10^{19} eV. The number of events above 10^{20} eV is 2.8 ± 1.4 for the case $m = 2$ and 2.5 ± 1.5 for $m = 4$ (these numbers are for a homogeneous distribution of the sources).
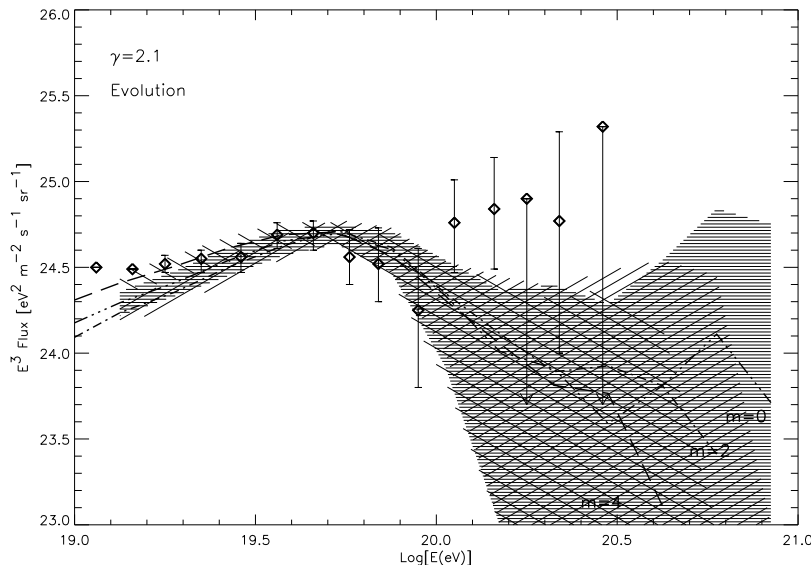

Fig. 8. *Simulated fluxes for the AGASA statistics of 728 events above 10^{19} eV, and $\gamma = 2.1$, using a homogeneous source distribution with $z_{max} = 1$ and $m = 0$ (horizontal hatches), $m = 2$ (/ hatches), and $m = 4$ (\ hatches). The lines are the results of the analytical calculations, as in [6].*

In trying to bridge the gap between predicted and observed ultra-high energy fluxes, we should consider some additional unknowns that may affect the output spectrum. For instance, it is not clear how the extragalactic component we have considered above gets modified by a Galactic component at the highest energies. The spectrum of Galactic cosmic rays might extend up to $\sim 10^{19}$ eV or even to higher energies. If the Galactic component continues to higher energies with the same spectrum as the observed one at lower energies (i.e., $E^{-3.1}$), it will improve the agreement with the AGASA observations when combined with the extragalactic flux plotted in Figure 7. We do not have sufficient information about the Galactic contribution at such high energies to rule out this possibility.

Another aspect of this problem that should be considered is the effect of extragalactic magnetic fields. As shown in [25,26], a large scale magnetic field with strength $\sim 10^{-7}$ – 10^{-9} G can steepen the spectrum of the observed cosmic ray particles significantly. This effect would improve the agreement with the AGASA data. But as the diffusive limit is reached, the effect might go in the opposite direction: for instance, if the effective diffusion coefficient is too small, then the propagation time may be larger than the age of the universe for low energy particles generated beyond some distance, considerably reducing the cosmic ray horizon [27]. In other words a smaller portion of the universe would contribute to the observed flux, thus reducing it. The highest energy component of the spectrum should not be affected appreciably by diffusive propagation, since most of the particles with $E > 10^{20}$ eV originate in the local universe, where propagation is likely to be non-diffusive. A complete answer to this question awaits a full propagation code that includes the effects of a realistic model of extragalactic magnetic fields.

5 Conclusion

We have studied the effects on the spectrum of ultra-high energy cosmic rays of sources associated with a realistic model for the galaxy distribution provided by the PSCz and CfA2 catalogs. We considered different injection spectra and the possibility of luminosity evolution of UHECR sources with redshift. We showed that when the galaxy selection functions are properly accounted for, the local overdensity is not as large as found by [8]. Thus, the AGASA observations are *inconsistent* with the predicted flux above 10^{20} eV for soft injection spectra ($\gamma \simeq 3$).

We confirm that a local overdensity helps bridge the agreement between theory and observations but only (and only slightly) for hard injection spectra ($\gamma \simeq 2$). In this case, the observations are within 2σ of the predicted number of events, in agreement with the findings of [9]. Sources of UHECRs having a density field following that of galaxies are therefore consistent with present data only for hard injection spectra and, in this case, the GZK cutoff is not really a *cutoff* but a *feature* in the overall cosmic ray spectrum.

As future experiments such as the Pierre Auger Project [28], the High Resolution Fly's Eye [29], the Telescope Array [30], and the EUSO [31] and OWL [32] satellite experiments increase the number of events observed above 10^{20} eV, a better determination of the shape of the GZK feature will be obtained. The GZK feature will contain information both on the injection spectrum (i.e., γ) as well as the clustering properties of the sources. Given γ, the clustering properties, and the angular distribution of arrival directions, a population of sources might be identifiable. If associated with active galaxies or some other

specific class of astrophysical objects, the shape of the GZK feature can be further used to constrain intergalactic magnetic fields [33] as well as more exotic pieces of physics, such as violations of Lorentz invariance [34].

Alternatively, the gap between observed and predicted flux may widen as more data accumulates. This would indicate that astrophysical proton accelerators are unlikely sources of UHECRs. The added difficulty in reaching the extreme energies in astrophysical sources further justifies the search for alternative explanations. Future experiments will play a crucial role in settling this long standing mystery, through the determination of the cosmic ray flux, and arrival direction distribution, and the great discriminator: the composition at extremely high energies.

Acknowledgment

References

[1] M. Takeda et al., Phys. Rev. Lett. 81 (1998) 1163; M. Takeda et al. preprint astro-ph/9902239 (submitted to Astrophys. J.); N. Hayashida et al. Phys. Rev. Lett. 73 (1994) 3491; D. J. Bird et al. Astrophys J. 441 (1995) 144; Phys. Rev. Lett. 71 (1993) 3401; Astrophys. J. 424 (1994) 491; M. A. Lawrence, R. J. O. Reid and A. A. Watson, J. Phys. G. Nucl. Part. Phys. 17 (1991) 773; N. N. Efimov et al., Ref. Proc. International Symposium on *Astrophysical Aspects of the Most Energetic Cosmic Rays*, eds. M. Nagano and F. Takahara (World Scientific, Singapore, 1991), p. 20; D. Kieda et al., HiRes Collaboration, Proceeds. 26th ICRC Salt Lake (1999); J. Linsley, Phys. Rev. Lett. 10 (1963) 146.

[2] K. Greisen, Phys. Rev. Lett. 16 (1966) 748; G. T. Zatsepin and V. A. Kuzmin, Sov. Phys. JETP Lett. 4 (1966) 78.

[3] N. Hayashida et al. (2000)

[4] A. Olinto, Phys.Rept. 333-334 (2000) 329.

[5] P. Bhattacharjee and G. Sigl, Phys. Rept. 327 (2000) 109.

[6] V. Berezinsky and S. Grigorieva, Astron. Astroph. 199 (1988) 1.

[7] Berezinsky, V. S., and Grigorieva, S. I., *Proc. 16th. Int. Cosmic Ray Conf., Kyoto* 2 (1979) 81.

[8] G. A. Medina-Tanco, Proceedings of 26th ICRC, Salt Lake City, Utah, vol 4, 346 (1999); Medina Tanco, G. A., Astrophys. J. 510 (1999) 91.

[9] J. N. Bahcall and E. Waxman, hep-ph/9912326v2 (2000).

[10] V.S. Ptuskin, S.I. Rogovaya, & V.N. Zirakashvili, Proceedings of 26th ICRC, Salt Lake City, Utah, vol 4, 271 (1999).

[11] Branch, D. 1998, *ARA&A*, 36, 17

[12] Davis, M., & Huchra, J. 1982, *ApJ*, 254, 437

[13] Strauss, M. A., & Willick, J.A. 1995, Phys. Rep., 261, 271

[14] Huchra, J. P., Geller, M. J., & Corwin, Jr., H. G. 1995, *ApJ*, 70, 687

[15] Saunders, W., Sutherland, W. J., Maddox, S. J., Keeble, O., Oliver, S. J., Rowan-Robinson, M., McMahon, R. G., Efstathiou, G., Tadros, H., White, S. D. M., Frenk, C. S., Carraminana, A., Hawkins, M. R. S. 2000, submitted to *MNRAS*, preprint (astro-ph/0001117)

[16] Peebles, P. J. E. 1993, Principles of Physical Cosmology (Princeton, NJ: Princeton University Press)

[17] Hogg, D. W. 1999, astro-ph/9905116

[18] Peebles, P. J. E. 1980, The Large-Scale Structure of the Universe (Princeton, NJ: Princeton University Press)

[19] Efstathiou, G., Ellis, R. S., & Peterson, B. S. 1988, *MNRAS*, 232, 431

[20] Sandage, A., Tammann, G. A., & Yahil, A. 1979, *ApJ*, 232, 352

[21] V. S. Berezinsky, S.V. Bulanov, V. A. Dogiel, V. L. Ginzburg, and V. S. Ptuskin, Astrophysics of Cosmic Rays, (Amsterdam: North Holland, 1990).

[22] Achterberg et al. 1998 A. Achterberg, Y. A. Gallant, C. A. Norman, D. B. Melrose, astro-ph/9907060

[23] Takeda, M., et al., *Phys. Rev. Lett.* **81**, 1163 (1998).

[24] Hayashida, N., et al., Appendix to *Astrophys. J.* **522**, 225 (1999) (preprint astro-ph/0008102).

[25] P. Blasi and A. V. Olinto, 1999, Phys. Rev. D 59, 023001.

[26] G. Sigl, M. Lemoine, and P. Biermann, Astropart. Phys. 10 (1999) 141.

[27] T. Stanev, R. Engel, A. Muecke, R. J. Protheroe, J. P. Rachen, astro-ph/0003484.

[28] J. W. Cronin, Nucl. Phys. B. (Proc. Suppl.) 28B (1992) 213.

[29] S. C. Corbató et al., Nucl. Phys. B (Proc. Suppl.) 28B (1992) 36.

[30] M. Teshima et al., Nucl. Phys. B (Proc. Suppl.) 28B (1992) 169.

[31] see http://www.ifcai.pa.cnr.it/Ifcai/euso.html

[32] R. E. Streitmatter, Proc. of *Workshop on Observing Giant Cosmic Ray Air Showers from $> 10^{20}$ eV Particles from Space*, eds. J. F. Krizmanic, J. F. Ormes, and R. E. Streitmatter (AIP Conference Proceedings 433, 1997).

[33] E. Waxman and J. Miralda-Escude, Astrophys. J. 472 (1996) L89; G. A. Medina Tanco, E. M. de Gouveia Dal Pino, and J. E. Horvath, Astropart. Phys. 6 (1997) 337; G. Sigl, M. Lemoine, and A. V. Olinto, Phys. Rev. 56 (1997) 4470; M. Lemoine, G. Sigl, A. V. Olinto, and D. Schramm, Astropart. Phys. 486 (1997) L115; G. Sigl, M. Lemoine, and P. Biermann, Astropart. Phys. 10 (1999) 141; D. Ryu, H. Kang and P. L. Bierman, Astron. Astrophys. 335 (1998) 19.

[34] L. Gonzalez-Mestres, Nucl. Phys. B (Proc. Suppl.) 48 (1996) 131; S. Coleman and S. L. Glashow, Phys. Rev. D 59 (1999) 116008; H. Sato and T. Tati, Prog. Theor. Phys. 47 (1972) 1788; D. A. Kirzhnits and V. A. Chechin, Sov. J. Nucl. Phys. 15 (1972) 585; R. Aloisio, P. Blasi, P Ghia, and A. Grillo, preprint INFN/AE-99/24.